Mendeleev Communications

Mendeleev Commun., 2025, **35**, 196–198

A universal method for preparing highly dispersed bimetallic nanoparticles: the case of Pd–Fe

Semyon A. Gulevich,[a] Mariya P. Shcherbakova-Sandu,*[a] Eugene P. Meshcheryakov,[a] Aleksandr V. Chernyavskii[b] and Irina A. Kurzina[a]

[a] *National Research Tomsk State University, 634050 Tomsk, Russian Federation. E-mail: mpsandu94@gmail.com*
[b] *M. V. Lomonosov Institute of Fine Chemical Technologies, MIREA – Russian Technological University, 119454 Moscow, Russian Federation*

DOI: 10.71267/mencom.7600

A new approach to the synthesis of highly dispersed deposited bimetallic Pd–Fe nanoparticles with a median size of 3–4 nm and a narrow size distribution has been developed, based on the use of metal acetylacetonates as starting materials. It has been established that Pd in the presence of Fe undergoes strong oxidation compared to monometallic nanoparticles. Comparison of the obtained results with data for other systems has shown the universality of the method for preparing highly dispersed palladium-based bimetallic nanoparticles.

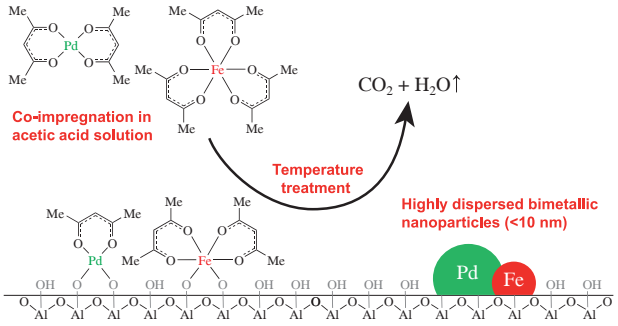

Keywords: bimetallic, palladium, supported nanoparticles, acetylacetonates, aluminum oxide.

Palladium nanoparticles are efficient catalyst systems that are widely used in a variety of industrial processes.[1–3] Pd has a lower cost than Pt and is characterized by a unique electronic structure ($4d^{10}$, $5s^0$), which can be strongly influenced by introducing an additional metal into the coordination environment.[4] The main advantage of bimetallic nanoparticles (BNPs) is the improvement of metal properties due to the paired synergistic effect.[5] Palladium-based bimetallic catalysts have attracted increasing attention due to their enhanced activity and stability.[6,7] Pd–Fe BNPs are promising catalysts that exhibit excellent activity in the cleavage of C–O and C–C bonds in biomass-derived cellulose, hemicellulose and lignin. They show high efficiency in important 'green' reactions: aqueous phase reforming, hydrogenolysis of C_2–C_6 polyols and furfural, and hydrodeoxygenation of phenol derivatives.[8] The most important parameter of BNPs is their size, and the enhanced properties are most pronounced in nanoparticles <10 nm. However, these metal particles are thermodynamically unstable, so when in solution, such particles merge into large agglomerates. One of the ways to stabilize BNPs is to deposit them on an inert support.[9]

In previous studies of Pd–Bi and Pd–Sn catalysts,[10,11] our research group used a new method for preparing highly dispersed supported BNPs of the mentioned composition based on the employment of organometallic precursors, *viz.* acetylacetonates.[12] However, the possibility of extending this method to other bimetallic systems has not been given enough attention. The present work was aimed to develop a new unique approach for preparing highly dispersed Pd–Fe BNPs from alumina-supported acetylacetonates.[†]

The materials were characterized by XRF, TEM, SEM, EDX, XPS, XRD and low-temperature N_2 adsorption–desorption methods[†] and the obtained data were compared with previous results for supported Pd–Bi and Pd–Sn BNPs to substantiate the versatility of the method.

Formation of Pd–Bi and Pd–Sn BNPs on the Al_2O_3 surface was considered earlier.[10,11] The formation process follows a similar mechanism and can be adapted to a wide range of BNPs formed by this method. At the stage of impregnation of the support with a solution of $Pd(acac)_2$ and $Fe(acac)_3$ precursors, the formation of surface-adsorbed acetylacetonate complexes presumably occurs due to the interaction with the coordinatively unsaturated centers of Al_2O_3 with the formation of intermediate acetylacetonate complexes [reactions (1) and (2)]. At the stage of calcination in an Ar atmosphere, the adsorbed complexes decompose with the formation of acetone [reactions (3)–(5)]. In addition, at this stage, dispersion of metals occurs, which covalently bind to the support after ligand decomposition.[14] Treatment in an O_2 flow is responsible for the oxidation reactions of acetone and metals [reactions (6)–(8)]. Hydrogen treatment results in the reduction of PdO and Fe_xO_y to their metallic forms [reactions (9) and (10)].

$$Pd(acac)_2 + (Al^{3+})_s \rightarrow [Al(acac)]_s^{2+} + [Pd(acac)]_s^{+} \quad (1)$$

$$Fe(acac)_3 + (Al^{3+})_s \rightarrow [Al(acac)]_s^{2+} + [Fe(acac)_2]_s^{+} \quad (2)$$

$$[Al(acac)]_s^{2+} \rightarrow [Al–O]_s + Me–CO–Me \quad (3)$$

[†] In a typical synthesis, γ-Al_2O_3 (125–250 μm fraction) was dried in a vacuum oven for 24 h at 120 °C and stirred in an acetic acid solution (200 ml) of the $Pd(acac)_2$ and $Fe(acac)_3$ precursors at 500 rpm for 20 h. The Pd/Fe atomic ratio was chosen to be 3 : 1, 10 : 1 and 20 : 1. The total metal content was approximately 6%. Excess solvent was removed using a rotary evaporator, followed by drying the samples in a vacuum cabinet at $T = 80$ °C. The resulting powder was subjected to successive temperature treatments for 2 h in an Ar atmosphere at 525 °C (to decompose the organometallic complexes), in an O_2 atmosphere at 375 °C (to remove organics) and in an H_2 atmosphere at 525 °C (to reduce PdO species).[13] The heating rate during the Ar treatment was 0.7 °C min^{-1} to ensure complete decomposition of metal acetylacetonates and 1.0 °C min^{-1} during the O_2 and H_2 treatment.

A description of the instrumental methods and the results of XRD, SEM, XPS and low-temperature N_2 desorption–adsorption studies are presented in Online Supplementary Materials.

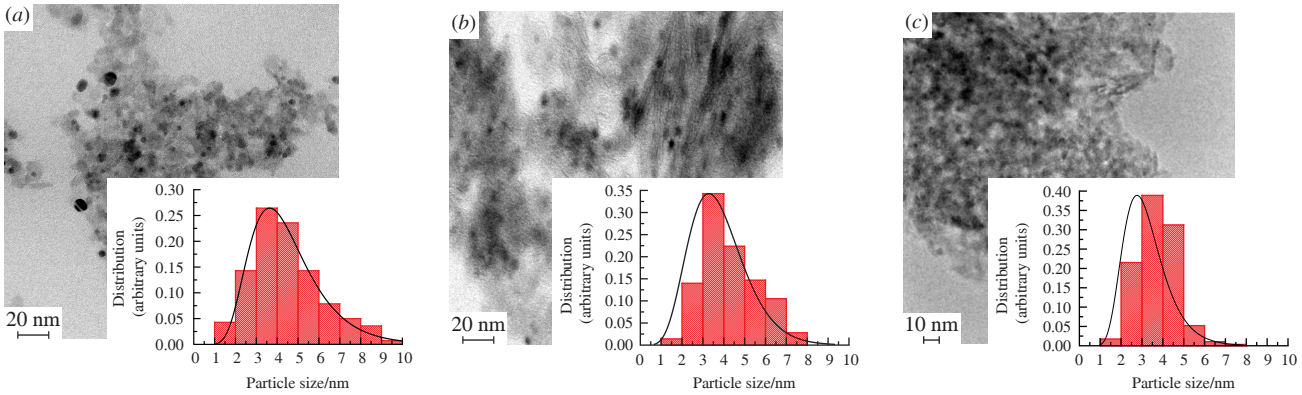

Figure 1 TEM micrographs and particle size distribution histograms for (*a*) 3Pd-1Fe, (*b*) 3Pd-1Bi (adapted from ref. 11) and (*c*) 3Pd-1Sn (adapted from ref. 10) samples.

$$[Pd(acac)]^{+}_{s} \rightarrow (Pd^{2+})_{s} + Me–CO–Me \quad (4)$$

$$[Fe(acac)_2]^{+}_{s} \rightarrow (Fe^{3+})_{s} + Me–CO–Me \quad (5)$$

$$Me–CO–Me + O_2 \rightarrow CO_2 + H_2O \quad (6)$$

$$(Pd^{2+})_{s} + O_2 \rightarrow (PdO)_{s} \quad (7)$$

$$(Fe^{3+})_{s} + O_2 \rightarrow (Fe_xO_y)_{s} \quad (8)$$

$$(PdO)_{s} + H_2 \rightarrow (Pd^{0}) + H_2O \quad (9)$$

$$(Fe_xO_y)_{s} + H_2 \rightarrow (Fe^{0}) + H_2O \quad (10)$$

The metal content in the samples was determined by XRF analysis (Table 1). The Pd/Fe ratios are close to those theoretically calculated.

The textural characteristics of the support do not undergo significant changes upon the deposition of BNPs, except for a slight decrease in the average pore diameter and volume, which may indicate partial adsorption in the large pores of alumina (Table S1, see Online Supplementary Materials). SEM micrographs are representative and demonstrate significant destruction of the initial fraction of the support during the synthesis [Figure S1(*a*), see Online Supplementary Materials]. The obtained samples have a fraction of up to 50 μm. EDX mapping showed a uniform distribution of metals on the alumina surface [Figure S1(*b*),(*c*)]. Rare inclusions of large Pd agglomerates are formed at the high-temperature treatment stage. Elemental analysis in several areas of the 3Pd-1Fe sample showed that the average Pd/Fe atomic ratio is 2.9 (Table S2), which coincides with the theoretically calculated one.

The XRD patterns for both the support and the H_2-pretreated Pd–Fe samples demonstrate primarily the main diffraction peaks of γ-Al_2O_3 (Figure S2). The growing peaks at 2θ of 40.2° and 46.7° confirm the formation of a well-crystallized Pd^0 phase.[15] However, no Fe phase and other Pd phases were detected in the XRD patterns, probably due to the small crystallite sizes and low metal content relative to the support.

TEM micrographs of the obtained samples demonstrate that the metal particles are well dispersed on the support surface [Figure 1(*a*)]. The particle shape is close to spherical. However, at a high Fe content (3Pd-1Fe), large agglomerates with an octahedral shape characteristic of iron oxides are formed.[16] For comparison, images of Pd–Bi and Pd–Sn samples with a ratio of 3 : 1 are shown [Figure 1(*b*),(*c*)].[10,11] The corresponding distribution histograms show rather narrow particle distributions with the main fraction of particles ranging in size from 2 to 6 nm. The character of the histograms corresponds to a lognormal distribution with a median value of approximately 3–4 nm for all samples. This indicates the possibility of preparing deposited monodisperse BNPs by this method regardless of the choice of the doping metal.

Table 1 Metal content in Pd–Fe/Al_2O_3 determined by XRF analysis.

Sample	Pd (wt%)	Fe (wt%)	Pd + Fe (wt%)	Pd/Fe (at/at)
3Pd-1Fe	5.9	0.9	6.8	3.2
10Pd-1Fe	6.6	0.3	6.9	10.9
20Pd-1Fe	6.3	0.2	6.5	19.6

To study the nature of the interaction between Pd and Fe, elemental mapping of the particles was carried out, which confirmed the close localization of Pd and Fe (Figure 2). Similar results are observed for all investigated samples of the Pd–Fe composition. A similar pattern was previously revealed for deposited Pd–Sn and Pd–Bi BNPs.[10,11]

The electronic state of Pd on the surface was studied by XPS. Monometallic Pd/Al_2O_3 was prepared as a reference sample for comparison. The XPS spectra for the Pd 3*d* core levels of all synthesized samples after the last pretreatment step in H_2 atmosphere (at 525 °C for 2 h) are presented in Figure 3. Two asymmetric peaks separated by 5.3 eV were found in the 3*d* spectrum of the palladium core, assigned to the Pd $3d_{5/2}$ and Pd $3d_{3/2}$ levels. The Pd $3d_{5/2}$ signals can be deconvoluted into two peaks: one centered at 335.2 eV, attributed to the metallic form of Pd^0, and the second peak centered at 336.4 eV, associated with the presence of the adsorbed oxidized form of Pd^{II}_{ads}.[17] The peak area ratio in the doublet is 3 : 2 in accordance with the spin–spin coupling law for *d*-elements and coincides with the deconvolution results (Table S3). The shift of Pd^{II} and Pd^0 toward lower binding energies indicates the presence of electronic interaction between Pd and Fe. It was observed that the addition of iron in a significant amount (3Pd-1Fe) leads to the formation of a fully oxidized state of palladium Pd^{II}(~45%) presumably due to the strong interaction between Pd and Fe, which is almost always in the oxidized state in air. A decrease in the amount of added iron promotes the formation of the Pd^{II}_{ads} form bound to the oxygen-containing groups of the support. At the same time, the content of the reduced Pd^0 form increases with decreasing iron content (20Pd-1Fe) due to the weakening of the electronic interaction between the metals. The formation of the Pd–O–Fe phase also cannot be excluded.[18]

Although the valence state was investigated after the reducing treatment of the samples, a high contribution of the oxidized

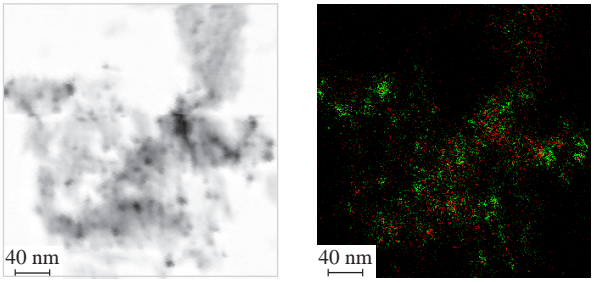

Figure 2 EDX mapping of the 3Pd-1Fe sample (Pd – green, Fe – red).

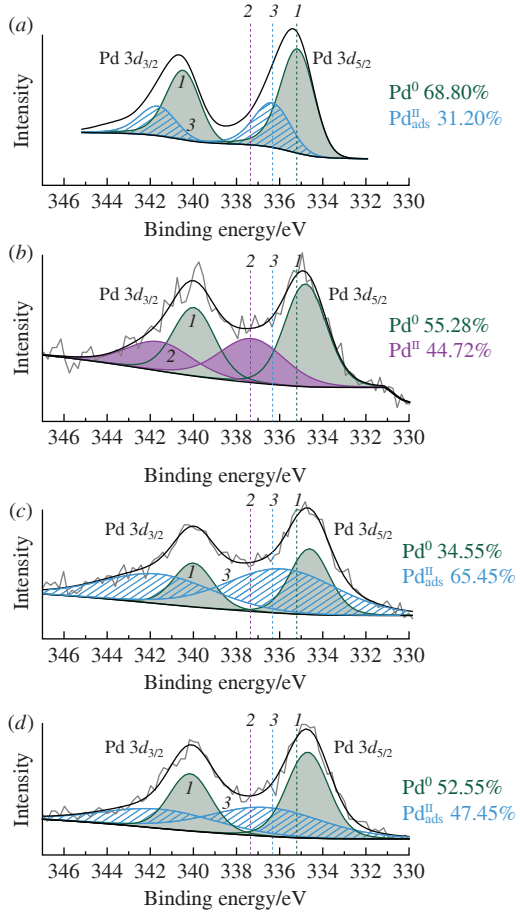

Figure 3 XPS spectra of Pd 3*d* core levels for (*a*) Pd, (*b*) 3Pd-1Fe, (*c*) 10Pd-1Fe and (*d*) 20Pd-1Fe samples. The signals were deconvoluted with contributions from (*1*) Pd^0, (*2*) Pd^{II} and (*3*) Pd^{II}_{ads} (shown as relative percentages).

form, which is not typical for monometallic Pd, is observed for all Pd–Fe samples. This effect is partly due to the interaction of Pd with oxygen species from alumina,[19] as in the case of monometallic Pd. However, Pd in the Pd–Fe samples is oxidized to a significantly higher extent than in Pd–Bi and Pd–Sn.[10,11] This feature is probably explained by the high affinity of Fe and, consequently, Pd–Fe BNPs for oxygen.

In conclusion, a novel approach to the synthesis of Al_2O_3-supported Pd–Fe BNPs has been developed. This method enables the preparation of supported BNPs with a median size of 3–4 nm regardless of the selected dopant metal by using acetylacetonates as organometallic precursors. At the same time, the nature of the particles formed and the electronic state of the alloy components depend on the nature of the added metal, which determines the functional properties. In the case of Pd–Fe, we observed a high content of the oxidized form of Pd compared to Pd–Bi and Pd–Sn.

This work was supported by the Ministry of Science and Higher Education of the Russian Federation (grant no. 075-15-2023-468).

Online Supplementary Materials

Supplementary data associated with this article can be found in the online version at doi: 10.71267/mencom.7600.

References

1 R. Grigg and S. P. Mutton, *Tetrahedron*, 2010, **66**, 5515; https://doi.org/10.1016/j.tet.2010.03.090.
2 M. Pagliaro, V. Pandarus, R. Ciriminna, F. Béland and P. Demma Carà, *ChemCatChem*, 2012, **4**, 432; https://doi.org/10.1002/cctc.201100422.
3 E. Antolini, *Energy Environ. Sci.*, 2009, **2**, 915; https://doi.org/10.1039/b820837a.
4 F. Liao, T. W. B. Lo and S. C. E. Tsang, *ChemCatChem*, 2015, **7**, 1998; https://doi.org/10.1002/cctc.201500245.
5 M. Gale, C. M. Cai and K. L. Gilliard-Abdul-Aziz, *ChemSusChem*, 2020, **13**, 1947; https://doi.org/10.1002/cssc.202000002.
6 P. V. Markov, I. S. Mashkovsky, G. N. Baeva, D. P. Melnikov and A. Yu. Stakheev, *Mendeleev Commun.*, 2023, **33**, 836; https://doi.org/10.1016/j.mencom.2023.10.032.
7 A. A. Shesterkina, V. S. Zhuravleva, K. E. Kartavova, A. A. Strekalova, K. V. Vikanova and A. L. Kustov, *Mendeleev Commun.*, 2024, **34**, 569; https://doi.org/10.1016/j.mencom.2024.06.033.
8 C. Espro, B. Gumina, E. Paone and F. Mauriello, *Catalysts*, 2017, **7**, 78; https://doi.org/10.3390/catal7030078.
9 P. Mäki-Arvela and D. Yu. Murzin, *Appl. Catal., A*, 2013, **451**, 251; https://doi.org/10.1016/j.apcata.2012.10.012.
10 I. Bondarchuk, F. J. Cadete Santos Aires, G. Mamontov and I. Kurzina, *Crystals*, 2021, **11**, 444; https://doi.org/10.3390/cryst11040444.
11 M. P. Sandu, M. A. Kovtunov, V. S. Baturin, A. R. Oganov and I. A. Kurzina, *Phys. Chem. Chem. Phys.*, 2021, **23**, 14889; https://doi.org/10.1039/d1cp01305j.
12 M. Benkhaled, S. Morin, Ch. Pichon, C. Thomazeau, C. Verdon and D. Uzio, *Appl. Catal., A*, 2006, **312**, 1; https://doi.org/10.1016/j.apcata.2006.06.011.
13 C. Méthivier, J. Massardier and J. C. Bertolini, *Appl. Catal., A*, 1999, **182**, 337; https://doi.org/10.1016/s0926-860x(99)00026-5.
14 A. R. Mouat, C. L. Whitford, B.-R. Chen, S. Liu, F. A. Perras, M. Pruski, M. J. Bedzyk, M. Delferro, P. C. Stair and T. J. Marks, *Chem. Mater.*, 2018, **30**, 1032; https://doi.org/10.1021/acs.chemmater.7b04909.
15 A. A. Shesterkina, L. M. Kozlova, I. V. Mishin, O. P. Tkachenko, G. I. Kapustin, V. P. Zakharov, M. S. Vlaskin, A. Z. Zhuk, O. A. Kirichenko and L. M. Kustov, *Mendeleev Commun.*, 2019, **29**, 339; https://doi.org/10.1016/j.mencom.2019.05.034.
16 A. P. Shcherban, G. P. Kovtun, D. A. Solopikhin, Y. V. Gorbenko, I. V. Kolodiy and V. D. Virich, *East European Journal of Physics*, 2020, **3**, 39; https://doi.org/10.26565/2312-4334-2020-3-05.
17 M. P. Sandu, M. S. Syrtanov, S. A. Orlov and I. A. Kurzina, *New J. Chem.*, 2023, **47**, 719; https://doi.org/10.1039/D2NJ03651G.
18 N. S. Babu, N. Lingaiah, J. V. Kumar and P. S. S. Prasad, *Appl. Catal., A*, 2009, **367**, 70; https://doi.org/10.1016/j.apcata.2009.07.031.
19 M. C. Valero, P. Raybaud and P. Sautet, *J. Catal.*, 2007, **247**, 339; https://doi.org/10.1016/j.jcat.2007.02.014.

Received: 23rd August 2024; Com. 24/7600